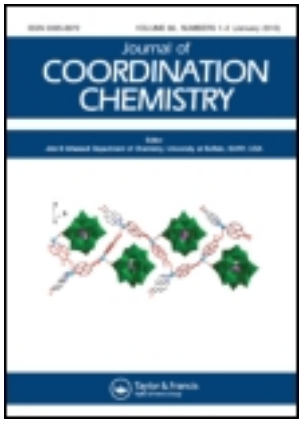

Journal of Coordination Chemistry
Publication details, including instructions for authors and subscription information:
http://www.tandfonline.com/loi/gcoo20

A twofold interpenetrating 3D Keggin-based Ag(I) complex based on a flexible bis-pyridyl-bis-amide

Xiuli Wang [a], Chuang Xu [a], Hongyan Lin [a], Guocheng Liu [a], Jian Luan [a], Zhihan Chang [a] & Aixiang Tian [a]

[a] Department of Chemistry, Liaoning Province Silicon Materials Engineering Technology Research Centre, Bohai University, Jinzhou, P.R. China

Accepted author version posted online: 12 Mar 2013.Published online: 15 Apr 2013.

To cite this article: Xiuli Wang, Chuang Xu, Hongyan Lin, Guocheng Liu, Jian Luan, Zhihan Chang & Aixiang Tian (2013) A twofold interpenetrating 3D Keggin-based Ag(I) complex based on a flexible bis-pyridyl-bis-amide, Journal of Coordination Chemistry, 66:8, 1451-1458, DOI: 10.1080/00958972.2013.783697

To link to this article: http://dx.doi.org/10.1080/00958972.2013.783697

Journal of Coordination Chemistry, 2013
Vol. 66, No. 8, 1451–1458, http://dx.doi.org/10.1080/00958972.2013.783697

A twofold interpenetrating 3D Keggin-based Ag(I) complex based on a flexible bis-pyridyl-bis-amide

XIULI WANG*, CHUANG XU, HONGYAN LIN, GUOCHENG LIU, JIAN LUAN, ZHIHAN CHANG and AIXIANG TIAN

Department of Chemistry, Liaoning Province Silicon Materials Engineering Technology Research Centre, Bohai University, Jinzhou, P.R. China

(*Received 24 October 2012; in final form 17 January 2013*)

A Keggin-type polyoxometalate (POM)-based complex, $[Ag_5(L)_3(HSiW_{10}^{VI}W_2^{V}O_{40})(H_2O)_2]\cdot 6H_2O$ (**1**) (L = N,N′-bis(3-pyridinecarboxamide)-1,2-ethane), has been hydrothermally synthesized. Compound **1** shows a 3D + 3D interpenetrating network with a (3,4,4,4)-connected $(4 \times 6^2)_2(4^2 \times 6^2 \times 8^2)(6^5 \times 8)_2$ topology, and it represents the first example of interpenetrating POM-based complex based on flexible bis-pyridyl-bis-amide ligands. Moreover, the electrochemical behavior and luminescence of **1** have been investigated.

Keywords: Keggin polyoxometalate; Metal-organic complex; Interpenetrating network; Flexible bis-pyridyl-bis-amide ligand

1. Introduction

Entangled systems have attracted interest not only for their intriguing architectures and topologies but also their promising applications as functional solid state materials [1–5]. Of the various types of entanglements in polymeric architectures, interpenetrating networks are the most studied [6–10]. Polyoxometalates (POMs), as a unique class of metal-oxide clusters and excellent inorganic building blocks, possess abundant structural diversity and versatile properties, such as photochemical activity, reversible redox behavior, and catalytic activity [11–16], and also possess a large number of potential coordination sites, thus can coordinate with metal-organic complexes to construct various architectures with attractive topologies and high dimensionality [17–19]. However, interpenetrating networks based on POM-building blocks and metal-organic complexes have been reported rarely [20–22]. It remains a challenge to construct high-dimensional POM-based interpenetrating structures.

Selection of organic ligands is extremely important for construction of interpenetrating architectures. Long organic ligands were frequently used to form networks with interpenetrating character [23–25]. The flexible bis-pyridyl-bis-amide, N,N′-bis(3-pyridinecarboxamide)-1,2-ethane (L) attracts our attention based on the following considerations:

*Corresponding author. Email: wangxiuli@bhu.edu.cn

(i) the pyridyl and amide could offer potential coordination sites; (ii) the $-(CH_2)_2-$ spacer and amide can enhance its flexibility and length, giving networks with big voids, which may provide interpenetration.

Based on the above considerations, we choose $H_4SiW_{12}O_{40}\cdot 26H_2O$, $AgNO_3$, and L as starting materials. As expected, a POM-based complex with twofold interpenetrating 3D + 3D network, $[Ag_5(L)_3(HSiW^{VI}_{10}W^{V}_{2}O_{40})(H_2O)_2]\cdot 6H_2O$, was obtained. To the best of our knowledge, it represents the first twofold interpenetrated 3D POM-based metal-organic framework based on a flexible bis-pyridyl-bis-amide ligand (scheme 1).

2. Experimental

2.1. *Materials and methods*

All reagents and solvents for syntheses were purchased from commercial sources and used as received without purification. L was prepared according to the literature method [26, 27]. FT-IR spectra (KBr pellets) were taken on a Magna FT-IR 560 Spectrometer. Elemental analyses (C, H, and N) were carried out on a Perkin-Elmer 240C elemental analyzer. Thermogravimetric (TG) analysis was performed on a SDT 2960 Simultaneous DSC-TGA instrument under flowing N_2 with a heating rate of $10\,^{\circ}C\,min^{-1}$. A CHI 440 Electrochemical Quartz Crystal Microbalance was used for electrochemical experiments. A conventional three-electrode cell was used at room temperature. The title compound bulk-modified carbon-paste electrode (CPE) was used as the working electrode. A saturated calomel electrode and a platinum wire were used as reference and auxiliary electrodes, respectively. The bulk modified CPEs were fabricated as from the literature [28]. Fluorescence spectra were performed on a Hitachi F-4500 fluorescence/phosphorescence spectrophotometer at room temperature.

2.2. *Preparation of the compound*

A mixture of $H_4SiW_{12}O_{40}\cdot 26H_2O$ (0.2 g, 0.07 mmol), $AgNO_3$ (0.085 g, 0.5 mmol), and L (0.027 g, 0.1 mmol) was dissolved in water (10 mL) at room temperature. The pH of the mixture was adjusted to about 3.5 with $1.0\,mol\,L^{-1}$ $NH_3\cdot H_2O$, then sealed in a 23 mL Telfon reactor and heated at 120 °C for 6 days. After slow cooling to room temperature, yellow block crystals were filtered and washed with distilled water. Yield: 28% based on Ag. Anal. Calcd. for $C_{42}H_{59}Ag_5N_{12}O_{54}SiW_{12}$ (4369.64): C, 11.53; H, 1.35; N, 3.84%. Found: C, 11.06; H, 1.41; N, 3.98%. IR (KBr pellet, cm^{-1}): 3336 (s), 1653 (s), 1600 (m), 1541 (s), 1458 (s), 1298 (m), 954 (s), 916 (s), 800 (s), 702 (w).

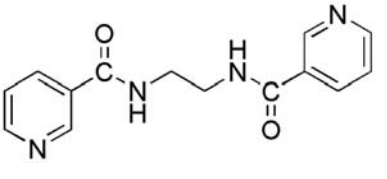

Scheme 1. The flexible bis-pyridyl-bis-amide, N,N′-bis(3-pyridinecarboxamide)-1,2-ethane (L).

2.3. *X-ray crystallographic study*

Crystallographic data for **1** were collected on a Bruker Smart 1000 CCD diffractometer with Mo Kα radiation ($\lambda = 0.71073$ Å) by ω and θ scan mode at 293 K. The structure was solved by direct methods and refined on F^2 by full-matrix least squares using the SHELXL package [29]. All hydrogens attached to water were not located, but were included in the structure factor calculations. Detailed crystal data and structure refinement for **1** are given in table 1. Selected bond lengths and angles are listed in table S1. Crystallographic data for the structure reported in this paper have been deposited in the Cambridge Crystallographic Data Center with CCDC Number 897820.

3. Results and discussion

3.1. *Description of crystal structure for 1*

Single crystal X-ray diffraction analysis reveals that **1** contains five Ag(I) ions, three *L*, one $[HSiW_{10}^{VI}W_2^{V}O_{40}]^{5-}$ (SiW_{12}), two coordinated waters, and six lattice waters. The valence sum calculation [30] shows that the oxidation state of 10 tungstens is + VI and that of the remaining two tungstens is + V. All Ag ions are in the + I oxidation states. To balance the charge of the compound, a hydrogen proton is added. There are three crystallographically independent Ag(I) ions (Ag1, Ag2, and Ag3) (figure 1). Ag1 is four-coordinated by one pyridyl N from L, two terminal O from two SiW_{12} and one O from water in a pyramidal style. The bond distances and angles around Ag1 are 2.17(2) Å for Ag–N, 2.15(3)–2.80(3) Å for Ag–O, and 84.8(9)–143.9(9)° for O–Ag–O. Ag2 also has pyramidal coordination, coordinated by one pyridyl N of L and three carbonyl O from two *L*. Carbonyl O coordinating to metal centers has not been observed in POM-based complexes based on flexible bis-pyridyl-bis-amide ligands [31–33]. The

Table 1. Crystal data and structure refinement for **1**.

Formula	$C_{42}H_{59}Ag_5N_{12}O_{54}SiW_{12}$
Formula weight	4369.64
Crystal system	Triclinic
Space group	*P*–*1*
a (Å)	13.366(3)
b (Å)	13.531(3)
c (Å)	13.837(3)
α (°)	71.949(3)
β (°)	66.289(3)
γ (°)	63.079(2)
V (Å^3)	2017.8(7)
Z	1
D_{calc} (g/cm^3)	3.595
μ/mm^{-1}	18.328
F(000)	1963
θ_{max} (°)	25
R_{int}	0.0277
R_1[a] [$I > 2\sigma(I)$]	0.0658
wR_2[b] (all data)	0.1716
GOF	1.093
$\Delta\rho_{max}$ (e Å^{-3})	0.1073
$\Delta\rho_{min}$ (e Å^{-3})	0.0963

[a]$R_1 = \Sigma||F_o|-|F_c||/\Sigma|F_o|$; [b]$wR_2 = \Sigma[w(F_o^2F_c^2)^2]/\Sigma[w(F_o^2)^2]^{1/2}$

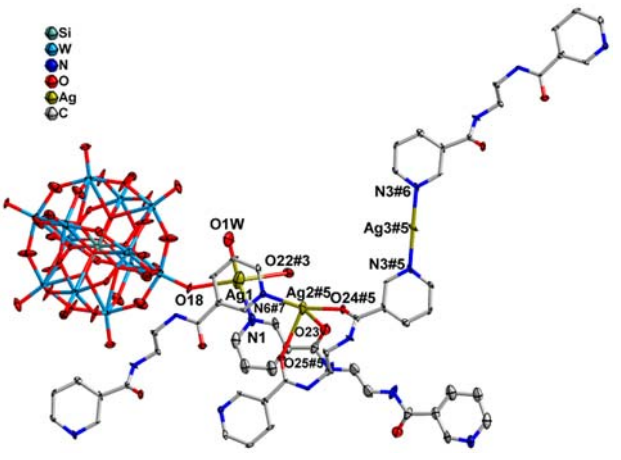

Figure 1. The coordination environment of Ag(I) in **1**. All hydrogens have been omitted for clarity (#3 −x+1, −y+1, −z+1; #5 x, y, 1+z; #6 1−x, 1−y, 2−z; #7 1−x, −y, 1−z).

bond distances and angles around Ag2 are 2.186(16) Å for Ag–N, 2.196(13)–2.786(13) Å for Ag–O, and 77.2(7)–110.5(7)° for O–Ag–O. Ag3 adopts linear geometry coordinated by two pyridyl N from two *L* with Ag–N distance of 2.088(18) Å and N–Ag–N angle of 179.999(2)°.

Two types of *L* (L_a and L_b) are observed in **1** (table S2 and figure S1). L_a shows GAG *cis* conformation and the dihedral angle between the two pyridyl rings is 8.28°. Two L_a utilize four carbonyl groups and two pyridyl groups chelating two Ag2 ions to form a $[Ag_2(L_a)_2]^{2+}$ subunit (figure S2). The $[Ag_2(L_a)_2]^{2+}$ subunits are further linked by Ag3 through another pyridyl N of L_a to generate a 1-D chain (figure S3). L_a is μ_3-bridging, providing two carbonyl O chelating one Ag2 and two pyridyl coordinating with one Ag3 and one Ag2, unprecedented in POM-based compounds containing flexible bis-pyridyl-bis-amides. In reported coordination polymers, flexible bis-pyridyl-bis-amides with μ_3-bridging coordination are very rare [34–36]. L_b is a μ_4-bridging ligand providing two carbonyl O to link two Ag2 ions from adjacent 1-D Ag-L_a chains and two pyridyls to coordinate with two Ag1 ions, adopting an AAA *trans* conformation with the dihedral angle between the two pyridyl rings of 0°. Thus, a 2D layer is generated (figure 2(a)). Furthermore, the 2D layers are ultimately extended to a 3D framework through SiW_{12} polyanions, which are tetradentate linking four

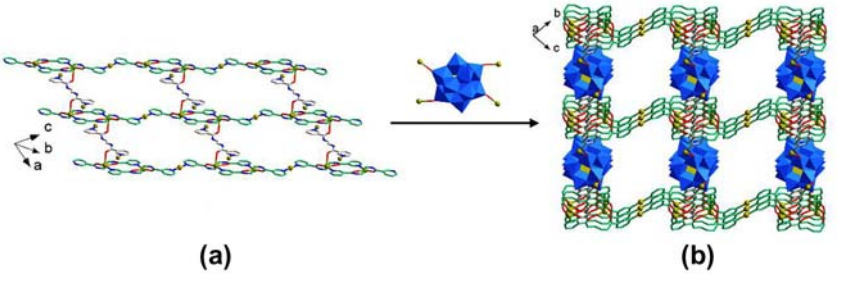

Figure 2. (a) The 2D structure of **1**; (b) The combined polyhedral and ball/stick representation of the 3D framework in **1**.

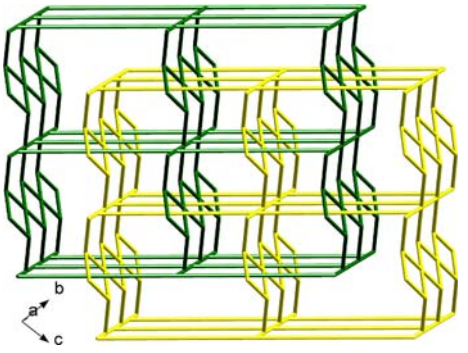

Figure 3. The topological representation of the twofold interpenetrating 3D + 3D network.

Ag1 ions (figure 2(b)). Moreover, there exists a channel with dimensions of 16.08×22.15 Å^2 (Ag3···Ag3 = 16.08 Å, Si1···Si1 = 22.15 Å).

If Ag1 is considered a 3-connected node, $[Ag_2(L_a)_2]^{2+}$ subunits and L_b and SiW_{12} polyanion are considered as 4-connected nodes, the structure of **1** is a (3,4,4,4)-connected framework with $(4\cdot6^2)_2(4^2\cdot6^2\cdot8^2)(6^5\cdot8)_2$ topology (figure S4). The large channel with dimensions of 16.08×22.15 Å^2 of **1** induces formation of the interpenetrating framework to stabilize the whole structure. Two sets of the same 3D frameworks interpenetrate with each other and an interesting twofold interpenetrating structure is formed (figure 3).

3.2. *IR spectrum*

The IR spectrum of **1** is shown in figure S5; the characteristic bands at 777, 885, and 956 cm^{-1} are attributed to ν(W–O$_c$–W), ν(W–O$_b$–W), and ν(W–O$_t$), respectively. The peaks at 922 and 1008 cm^{-1} are ascribed to ν(Si–O$_a$) [37–40]. Bands at 1653 and 1600 cm^{-1} are due to the stretch of C=O from L. Bands at 1541 and 1458 cm^{-1} suggest

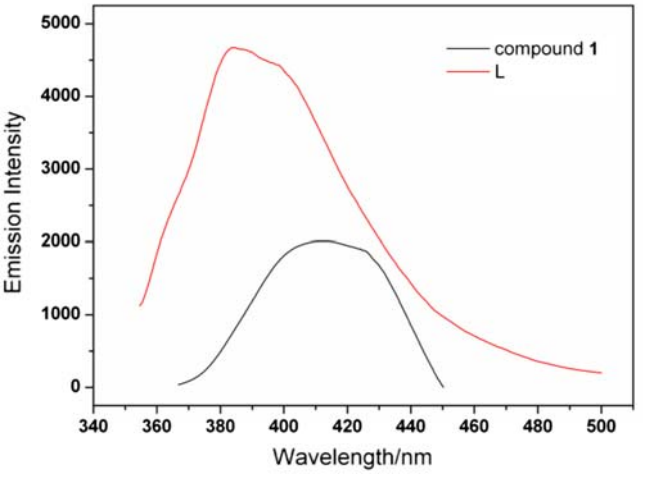

Figure 4. Emission spectra of L and **1** at room temperature.

ν_{C-N} of the pyridyl ring [41, 42]. The strong peak around 3400 cm^{-1} can be associated with the presence of water.

3.3. *Thermal gravimetric analysis*

The TG experiment was performed under N_2 with a heating rate of 10 °C min^{-1} from room temperature to 800 °C, as shown in figure S6. The TG curve of **1** shows two distinct weight loss steps: the first below 300 °C can be ascribed to loss of water 3.01% (Calcd 3.29%); the second weight loss corresponds to loss of organic molecules and one proton from $[HSiW_{10}^{VI}W_2^{V}O_{40}]^{5-}$ 19.20% (Calcd 18.56%).

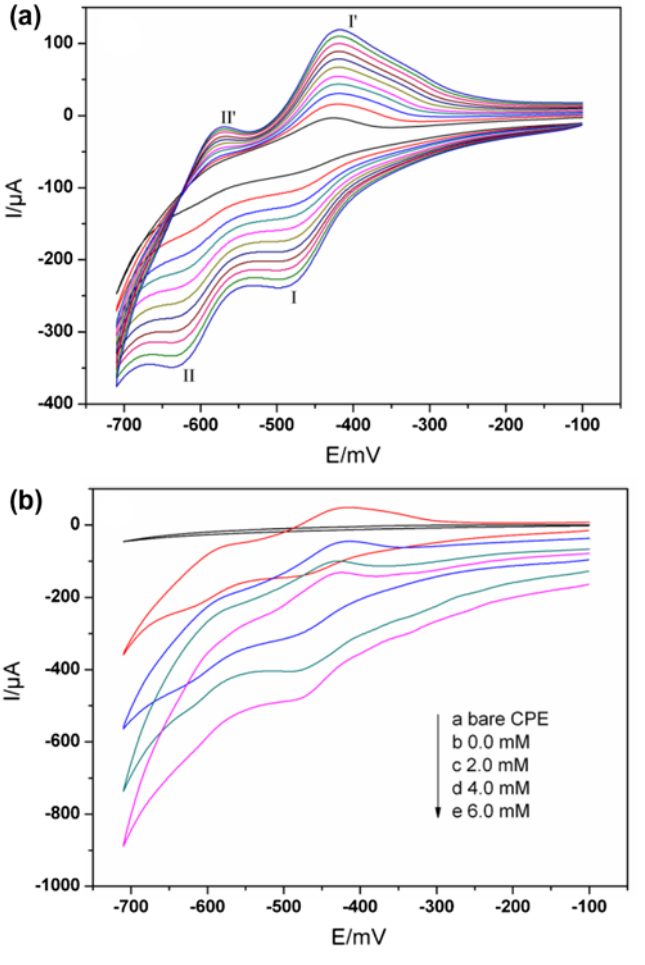

Figure 5. (a) The cyclic voltammograms of **1**-CPE in 1 M H_2SO_4 aqueous solution at different scan rates (from inner to outer: 40, 80, 120, 160, 200, 250, 300, 350, 400, 450, and 500 mV s^{-1}); (b) Cyclic voltammograms of **1**-CPE in 1 M H_2SO_4 aqueous solution containing 0.0–6.0 mM KNO_2 and a bare CPE in 4.0 mM KNO_2 + 1 M H_2SO_4 aqueous solution. Scan rate: 120 mV s^{-1}.

3.4. *Photoluminescent property*

Photoluminescent properties of **1** and free *L* were investigated in the solid state at room temperature. As shown in figure 4, *L* exhibits an emission at 385 nm upon excitation at 320 nm. The emission peak of *L* may be assigned to $\pi \rightarrow \pi^*$ transitions [35, 43]. Upon the same excitation, emission of **1** is at 415 nm, which is red-shifted compared with *L*. Therefore, the emission of **1** may be due to charge transfer transitions between the ligands and metals [44].

3.5. *Electrochemical behavior of 1-CPE*

The cyclic voltammetric behavior of **1** bulk-modified carbon paste electrode (**1**-CPE) in 1 M H_2SO_4 aqueous solution at different scan rates is presented in figure 5(a). There are two reversible redox peaks (I–I′, II–II′) from −710 to −100 mV, ascribed to redox of SiW_{12} [45, 46]. The mean peak potentials $E_{1/2} = (E_{pa} + E_{pc})/2$ are −462, −596 mV (120 mV s^{-1}). The peak potentials change gradually following the scan rates from 40 to 500 mV s^{-1}: cathodic peak potentials shift towards the negative direction and the corresponding anodic peak potentials to the positive direction with increasing scan rates. Peak currents are proportional to the scan rates (figure S7), indicating that the redox process of **1**-CPE is surface controlled.

The reduction of nitrite at most electrode surfaces requires a large overpotential and no obvious response was observed at a bare CPE [47]. However, **1**-CPE showed good electrocatalytic activity toward reduction of nitrite in 1 M H_2SO_4 aqueous solution. In the range of −710 to −100 mV (figure 5(b)), with the addition of nitrite, all the reduction peak currents gradually increase while the corresponding oxidation peak currents decrease, suggesting that all reduced species of SiW_{12} in **1** possess electrocatalytic activity toward the reduction of nitrite.

4. Conclusion

By using the flexible bis-pyridyl-bis-amide L, a SiW_{12}-based Ag(I) compound with a twofold interpenetrating 3D network has been synthesized and characterized. It represents the first example of interpenetrating POM-based complex based on flexible bis-pyridyl-bis-amide ligands. The **1**-CPE exhibits good electrocatalytic activity towards reduction of nitrite. The successful synthesis of **1** may provide a strategy to prepare new materials with novel structures and potential properties.

Acknowledgments

This work was supported by the Program for New Century Excellent Talents in University (NCET-09-0853), the National Natural Science Foundation of China (Nos. 21171025 and 21101015), Natural Science Foundation of Liaoning Province (No. 201102003), and Program of Innovative Research Team in University of Liaoning Province (LT2012020).

References

[1] S.J. Loeb. *Chem. Commun.*, **1511**, (2005).
[2] N.W. Ockwig, O.D. Friedrichs, M. O'Keeffe, O.M. Yaghi. *Acc. Chem. Res.*, **38**, 176 (2005).

[3] J.S. Miller. *Adv. Mater.*, **13**, 525 (2001).
[4] D.F. Sun, S.Q. Ma, Y.X. Ke, D.J. Collins, H.C. Zhou. *J. Am. Chem. Soc.*, **128**, 3896 (2006).
[5] Y.H. Xu, L. Chen, Z.Q. Guo, A. Nagai, D.L. Jiang. *J. Am. Chem. Soc.*, **133**, 17622 (2011).
[6] Y.E. Cheon, M.P. Suh. *Chem. Eur. J.*, **14**, 3961 (2008).
[7] N. Leventis, N. Chandrasekaran, A.G. Sadekar, C. Sotiriou-Leventis, H.B. Lu. *J. Am. Chem. Soc.*, **131**, 4576 (2009).
[8] M.C. Das, H. Xu, Z.Y. Wang, G. Srinivas, W. Zhou, Y.F. Yue, V.N. Nesterov, G.D. Qian, B.L. Chen. *Chem. Commun.*, **47**, 11715 (2011).
[9] Y. Gong, Y.C. Zhou, T.F. Liu, J. Lü, D.M. Proserpio, R. Cao. *Chem. Commun.*, **47**, 5982 (2011).
[10] Z.Z. Lu, R. Zhang, Z.R. Pan, Y.Z. Li, Z.J. Guo, H.G. Zheng. *Chem. Eur. J.*, **18**, 2812 (2012).
[11] C.L. Hill. *Chem. Rev.*, **98**, 1 (1998).
[12] D.L. Long, E. Burkholder, L. Cronin. *Chem. Soc. Rev.*, **36**, 105 (2007).
[13] C.Y. Sun, S.X. Liu, D.D. Liang, K.Z. Shao, Y.H. Ren, Z.M. Su. *J. Am. Chem. Soc.*, **131**, 1883 (2009).
[14] S.T. Zheng, G.Y. Yang. *Dalton Trans.*, **39**, 700 (2010).
[15] F.J. Ma, S.X. Liu, C.Y. Sun, D.D. Liang, G.J. Ren, F. Wei, Y.G. Chen, Z.M. Su. *J. Am. Chem. Soc.*, **133**, 4178 (2011).
[16] H. Fu, C. Qin, Y. Lu, Z.M. Zhang, Y.G. Li, Z.M. Su, W.L. Li, E.B. Wang. *Angew. Chem. Int. Ed.*, **51**, 7985 (2012).
[17] H.Y. An, E.B. Wang, D.R. Xiao, Y.G. Li, Z.M. Su, L. Xu. *Angew. Chem. Int. Ed.*, **45**, 904 (2006).
[18] X.L. Wang, C. Qin, E.B. Wang, Z.M. Su, Y.G. Li, L. Xu. *Angew. Chem. Int. Ed.*, **45**, 7411 (2006).
[19] Y.F. Bi, S.C. Du, W.P. Liao. *Chem. Commun.*, **47**, 4724 (2011).
[20] L.L. Fan, D.R. Xiao, E.B. Wang, Y.G. Li, Z.M. Su, X.L. Wang, J. Liu. *Cryst. Growth Des.*, **7**, 592 (2007).
[21] Y.M. Xie, R.M. Yu, X.Y. Wu, F. Wang, S.C. Chen, C.Z. Lu. *CrystEngComm*, **12**, 3490 (2010).
[22] P.P. Zhang, J. Peng, H.J. Pang, J.Q. Sha, M. Zhu, D.D. Wang, M.G. Liu, Z.M. Su. *Cryst. Growth Des.*, **11**, 2736 (2011).
[23] Y.Q. Lan, S.L. Li, X.L. Wang, K.Z. Shao, D.Y. Du, H.Y. Zang, Z.M. Su. *Inorg. Chem.*, **47**, 8179 (2008).
[24] X.L. Wang, H.Y. Lin, Y.F. Bi, B.K. Chen, G.C. Liu. *J. Solid State Chem.*, **181**, 556 (2008).
[25] X.D. Du, C.H. Li, Y. Zhang, S. Liu, Y. Ma, X.Z. You. *CrystEngComm*, **13**, 2350 (2011).
[26] S. Muthu, J.H.K. Yip, J.J. Vittal. *J. Chem. Soc., Dalton Trans.*, 3577 (2001).
[27] S. Muthu, J.H.K. Yip, J.J. Vittal. *J. Chem. Soc., Dalton Trans*., 4561 (2002).
[28] X.L. Wang, H.Y. Lin, B. Mu, A.X. Tian, G.C. Liu. *Dalton Trans.*, **39**, 6187 (2010).
[29] G.M. Sheldrick. *Acta Crystallogr., Sect. A*, 64, 112 (2008).
[30] I.D. Brown, D. *Altermatt. Acta Crystallogr., Sect. B*, 41, 244 (1985).
[31] H. Chen, H.Y. An, X. Liu, H.L. Wang, Z.F. Chen, H. Zhang, Y. Hu. *Inorg. Chem. Commun.*, **21**, 65 (2012).
[32] X.L. Wang, C. Xu, H.Y. Lin, G.C. Liu, S. Yang, Q. Gao, A.X. Tian. *CrystEngComm*, **14**, 5836 (2012).
[33] X.L. Wang, C. Xu, H.Y. Lin, G.C. Liu, J. Luan, A.X. Tian, J.W. Zhang. *Inorg. Chem. Commun.*, **24**, 43 (2012).
[34] M.J. Sie, Y.J. Chang, P.W. Cheng, P.T. Kuo, C.W. Yeh, C.F. Cheng, J.D. Chen, J.C. Wang. *CrystEngComm*, **14**, 5505 (2012).
[35] P.C. Cheng, C.W. Yeh, W. Hsu, T.R. Chen, H.W. Wang, J.D. Chen, J.C. Wang. *Cryst. Growth Des.*, **12**, 943 (2012).
[36] H.L. Hu, Y.F. Hsu, C.J. Wu, C.W. Yeh, J.D. Chen, J.C. Wang. *Polyhedron*, **33**, 280 (2012).
[37] A.X. Tian, X.L. Lin, Y.J. Liu, G.Y. Liu, J. Ying, X.L. Wang, H.Y. Lin. *J. Coord. Chem.*, **65**, 2147 (2012).
[38] R. Yang, S.X. Liu, Q. Tang, S.J. Li, D.D. Liang. *J. Coord. Chem.*, **65**, 891 (2012).
[39] J. Ying, M. Hou, X.J. Liu, A.X. Tian, X.L. Wang. *J. Coord. Chem.*, **65**, 218 (2012).
[40] J. Wu, C.X. Wang, K. Yu, Z.H. Su, Y. Yu, Y.L. Xu, B.B. Zhou. *J. Coord. Chem.*, **65**, 69 (2012).
[41] Y.F. Hsu, C.H. Lin, J.D. Chen, J.C. Wang. *Cryst. Growth Des.*, **8**, 1094 (2008).
[42] N.N. Adarsh, P. Dastidar. *Cryst. Growth Des.*, **11**, 328 (2011).
[43] Y.F. Hsu, H.L. Hu, C.J. Wu, C.W. Yeh, D.M. Proserpio, J.D. Chen. *CrystEngComm*, **11**, 168 (2009).
[44] H.Y. Liu, L. Bo, J. Yang, Y.Y. Liu, J.F. Ma, H. Wu. *Dalton Trans.*, **40**, 9782 (2011).
[45] J.Q. Sha, J. Peng, A.X. Tian, H.S. Liu, J. Chen, P.P. Zhang, Z.M. Su. *Cryst. Growth Des.*, **7**, 2535 (2007).
[46] M. Sadakane, E. Steckhan. *Chem. Rev.*, **98**, 219 (1998).
[47] B. Keita, L. Nadjo. *J. Electroanal. Chem.*, **227**, 77 (1987).